Two-photon ionization of the Ar atom and detachment of the F^- ion

Cheng Pan, Bo Gao, and Anthony F. Starace
Department of Physics and Astronomy, The University of Nebraska, Lincoln, Nebraska 68588-0111
(Received 5 February 1990)

Theoretical calculations of the two-photon ionization cross section of argon and of the two-photon detachment cross section of the negative fluorine ion are presented for the energy region from threshold to the single-photon ionization or detachment threshold. Detailed analyses are presented of the effects of various kinds of electron correlations, whose contributions to the two-photon transition amplitudes are evaluated using variationally stable procedures to sum implicitly over intermediate states. These variationally stable procedures enable us to give much more reliable predictions in the region of the first few intermediate-state resonances in argon than were provided by previous calculations of one of us [A.F. Starace and T. F. Jiang, Phys. Rev. A **36**, 1705 (1987)]. In addition, we show here for both argon and F^- the large corrections to the $p(^1S)$ final-state channel cross sections provided by certain intermediate-state shake-up interactions, which we show to be essential for obtaining good agreement of dipole length and velocity cross sections. We provide detailed comparisons of our results with those of previous workers; in particular, our results for the negative fluorine ion are in excellent agreement with the recent absolute measurement of Kwon *et al.* [Phys. Rev. A **40**, 676 (1989)].

I. INTRODUCTION

The explosive growth over the past decade in the number of experimental studies of intense laser-atom interactions has been a strong stimulus for corresponding theoretical studies on multiphoton ionization (MPI) processes.[1] In particular, the experimental observations of unusually large numbers of multiply charged ions produced by MPI of the rare gases[2,3] (among other targets), together with the interpretation that successive stages of ionization occur sequentially,[4] has led to a corresponding growth in the number of theoretical studies of low-order MPI processes for the rare gases.[5–15] This theoretical interest has extended also to negative ions which are isoelectronic to the rare gases, i.e., the negative hydrogen ion[16,17] and the negative halogen ions.[18–21] It has been stimulated further by recent wavelength-dependent experimental measurements of low-order MPI cross sections for the rare gases,[22,23] the negative hydrogen ion,[24] and the negative halogen ions.[25–27]

In every case, the theoretical calculations referred to above have confronted some key difficulties inherent in describing low-order MPI processes for the rare gases and the negative ions isoelectronic to them. First, there is the problem of maintaining numerical accuracy while summing over one or more complete sets of intermediate states. This problem is usually most severe in the neighborhood of intermediate-state resonances, which strongly influence MPI cross sections in the rare gases. A common theoretical procedure which avoids explicit summation over intermediate states is to solve instead an inhomogeneous differential equation.[28,29] The instability of the solutions of this inhomogeneous differential equation near intermediate-state resonances may be addressed by removing these resonances using projection operator techniques.[30] Their effect on the transition amplitude is then calculated separately. For all but the lowest-energy resonances, however, this procedure can be cumbersome.

A second problem is that of representing the atomic states realistically and, in particular, taking into account effects of electron correlations. For the negative halogen ions, Crance[19] has shown that the multiphoton detachment cross sections obtained using a plane-wave representation for the detached electron are often two to three times larger than those obtained using the more accurate LS-dependent Hartree-Fock representation for the detached electron. For the rare gases, a number of theoretical studies[6,9,10,12–14] have demonstrated that electron correlations can influence two-photon ionization cross sections by a factor of 2 or so, particularly near intermediate-state resonances. It is to be expected that such effects of electronic correlations will be magnified for higher-order MPI cross sections.

In this paper we address both of these difficulties by employing variationally stable procedures to obtain the two-photon ionization cross section for argon as well as the two-photon detachment cross section for F^-. These procedures are employed to calculate perturbation matrix elements which account in detail for effects of electron correlations, particularly in the vicinity of intermediate-state resonances (in the case of argon). The use of variational methods for the calculation of observables of second order in some perturbation, such as polarizabilities[31] and energy corrections,[32] has been common since the 1950s and more recently has been used for the calculation of second-order scattering amplitudes.[33] Most recently, Gao and Starace[34] introduced a new variational method for the calculation of perturbative processes of high order. Their calculations for multiphoton processes in atomic hydrogen of up to 11th order exhibited excellent numerical stability and accuracy even near

intermediate-state resonances.[34] The present work applies such variational methods to multiphoton processes involving nonhydrogenic targets.

In Sec. II we discuss the variationally stable methods we have used to calculate the most important electron correlation effects on the two-photon ionization cross section of Ar and the two-photon detachment cross section of F^-. We discuss, in particular, the accurate treatment of certain electron scattering interactions which have been found previously to affect significantly the two-photon ionization cross sections of argon[12] and xenon.[13] In addition, we discuss certain intermediate-state shake-up interactions, which we show to have a substantial influence on the $p(^1S)$ final-state channels. In Sec. III we present our results for argon. The variationally stable method we employ gives significantly improved predictions in the vicinity of the lowest-energy intermediate-state resonances as compared to a previous calculation by one of us,[12] which treated almost all of the electron correlation effects that we treat here. We also compare our length results with those of other authors.[6,8,9] In addition, we demonstrate the agreement of our length and velocity results and, in particular, show that shake-up interactions within the $p(^1S)$ final-state channel are very important for bringing velocity-form transition matrix elements into agreement with the corresponding length-form matrix elements. In Sec. IV we present similarly our results for F^- and include a comparison with previous theoretical work.[18,19] Once again, we find that shake-up interactions in the $p(^1S)$ channel must be included in order to obtain good agreement of length and velocity results. Our total cross-section results are shown to agree with a recent absolute experimental measurement.[27] In Sec. V we discuss our conclusions on our use of variationally stable methods to calculate multiphoton transition amplitudes with inclusion of electron correlation effects. A preliminary report of the present results has been given elsewhere.[35]

II. VARIATIONALLY STABLE CALCULATION OF TWO-PHOTON TRANSITION AMPLITUDES

For the many-electron systems we are interested in here, i.e., Ar and F^-, the calculation of two-photon transition amplitudes with the inclusion of electron correlation effects is complicated by the necessary summations over one or more infinite sets of intermediate states. Our general procedure is to enumerate the correlation effects we wish to include, then evaluate the angular factors exactly for the corresponding transition amplitudes (i.e., taking full account of the Pauli principle), and, finally, calculate the remaining radial amplitudes using variationally stable methods. In what follows. we enumerate the correlation effects we include in our calculations. We then illustrate the variationally stable procedures employed for several of the most important transition amplitudes.

A. Enumeration of electron correlation effects

For a two-photon ionization (detachment) process between an initial atomic (ionic) state $|i\rangle$ and a final state $\langle f|$, the transition amplitude is

$$T_{i\to f}^{(2)} \equiv \left\langle f \left| D \frac{1}{E_i+\omega-H} D \right| i \right\rangle . \tag{1}$$

Here H is the exact atomic (ionic) Hamiltonian, E_i is the energy of the initial state, ω is the photon frequency, and D is the electric dipole operator, which in length form is

$$D = \hat{\epsilon}_\alpha \cdot \sum_{i=1}^{N} \mathbf{r}_i , \tag{2}$$

where $\hat{\epsilon}_\alpha$ is the photon polarization unit vector and $\mathbf{r}_i$ is the coordinate vector of the ith atomic (ionic) electron. [It may be verified easily that the electric dipole operator in velocity form gives a result for the two-photon transition amplitude in Eq. (1) equal to that obtained by making the substitution $\mathbf{r}_i \to -i\mathbf{p}_i/\omega$ in Eq. (2), where $\mathbf{p}_i$ is the momentum operator for the ith electron and where ω is the photon frequency.[36]]

In Eq. (1), of course, $\langle f|$ and $|i\rangle$ are the exact final and initial states. A lowest-order approximation to the transition amplitude is obtained by employing the appropriate Hartree-Fock (HF) approximations for the initial and final states as well as for the Hamiltonian, i.e.,

$$T_{i\to f}^{(2)}(\mathrm{HF}) \equiv \left\langle f_{\mathrm{HF}} \left| D \frac{1}{E_i^{\mathrm{HF}}+\omega-H_{\mathrm{HF}}} D \right| i_{\mathrm{HF}} \right\rangle . \tag{3}$$

In our calculations for two-photon single ionization of the outer subshell of a rare-gas atom (or, equivalently, for two-photon detachment of a negative ion with a rare-gas electronic configuration), the appropriate HF representation for the initial and final states is straightforward:

$$|i_{\mathrm{HF}}\rangle \equiv |np^6(^1S)\rangle , \tag{4}$$

$$|f_{\mathrm{HF}}\rangle \equiv |np^5\epsilon l(^1L)\rangle . \tag{5}$$

In Eq. (4), the one-electron orbitals are the solutions of the usual HF equations for the atomic or ionic ground state.[37] In Eq. (5), the core orbitals are chosen as those of the initial state (i.e., we employ the frozen-core approximation). The radial wave function for the continuum electron, designated in Eq. (5) by ϵl, is obtained as the solution of the appropriate LS-dependent HF potential.[37,38] Use of the HF Green's function operator in Eq. (3) allows one either to carry out the summation over intermediate states explicitly or to evaluate it employing implicit summation techniques.[28,29]

Higher-order corrections to the lowest-order transition amplitude in Eq. (3) take account of electron correlation effects. Within the HF basis, these effects may occur in the initial, intermediate, or final states. To first order in the perturbation operator,

$$V \equiv \sum_{\substack{i,j \\ i>j}} \frac{1}{r_{ij}} - V_{\mathrm{HF}} ; \tag{6}$$

there are thus three types of higher-order corrections to the transition operator, viz.,

$$T^{(2)}_{i\to f}(V)\equiv\left\langle f_{\rm HF}\left|D\frac{1}{(E_i^{\rm HF}+\omega-H_{\rm HF})}D\frac{1}{(E_i^{\rm HF}-H_{\rm HF})}V\right|i_{\rm HF}\right\rangle$$
$$+\left\langle f_{\rm HF}\left|D\frac{1}{(E_i^{\rm HF}+\omega-H_{\rm HF})}V\frac{1}{(E_i^{\rm HF}+\omega-H_{\rm HF})}D\right|i_{\rm HF}\right\rangle$$
$$+\left\langle f_{\rm HF}\left|V\frac{1}{(E_i^{\rm HF}+\omega-H_{\rm HF})}D\frac{1}{(E_i^{\rm HF}+\omega-H_{\rm HF})}D\right|i_{\rm HF}\right\rangle . \quad (7)$$

To first order in V, then, the exact two-photon transition amplitude in Eq. (1) may be approximated by the sum of Eqs. (3) and (7),

$$T^{(2)}_{i\to f}\approx T^{(2)}_{i\to f}({\rm HF})+T^{(2)}_{i\to f}(V) . \quad (8)$$

Because of the way the HF potential is defined,[37,38] intrachannel matrix elements of V between singly excited states (i.e., matrix elements between singly excited states differing only in the energy of the excited electron) are zero. However, interchannel matrix elements of V between singly excited states (i.e., matrix elements between singly excited states differing not only in the energy of the excited electron but also in other quantum numbers) are generally nonzero. Furthermore, the two dipole operators D and the Coulomb operator,

$$\sum_{\substack{i,j\\ i>j}}\frac{1}{r_{ij}} ,$$

also lead to intermediate states in the amplitudes in Eq. (7) which have two or more excited electrons. Matrix elements of V between such states, or between such a doubly excited state and the ground state, are also generally nonzero.

In order to include such doubly excited intermediate states when calculating the amplitudes in Eq. (7), straightforward application of the variationally stable procedures of Gao and Starace[34] requires, in general, finite basis expansions in two of the electron radial coordinates. We have not employed such general double expansions in this paper. Rather we have taken a more *ad hoc* approach, judiciously choosing appropriate expansions for each of the amplitudes we have calculated, as described below.

The specific processes we have included in our calculations are listed schematically in Table I. This schematization is compact since distinctions regarding direct and exchange interactions as well as specific angular momentum coupling schemes are implicit. The table is ordered as follows: the lowest-order processes shown are those which contribute to the HF amplitude in Eq. (3); the pro-

TABLE I. Schematic listing of the transition amplitudes included in the present calculations for the two-photon ionization process, Ar $3p^6(^1S)+2\gamma\to Ar^+\ 3p^5(^2P)\epsilon l(^1L)$, and the two-photon detachment process, $F^-\ 2p^6(^1S)+2\gamma\to F\ 2p^5(^2P)\epsilon l(^1L)$.

Process	Schematic description[a]
(1) Lowest-order processes	(a) $p^6\xrightarrow{\gamma}p^5\epsilon_1 l_1\xrightarrow{\gamma}p^5\epsilon l$
	(b) $s^2p^6\xrightarrow{\gamma}sp^6\epsilon l\xrightarrow{\gamma}p^5\epsilon l$
(2) Intermediate-state interchannel interactions	$p^6\xrightarrow{\gamma}p^5\epsilon_1 l_1\xrightarrow{V}p^5\epsilon_2 l_2\xrightarrow{\gamma}p^5\epsilon l$
(3) Ground-state correlations	(a) $p^6\xrightarrow{V}p^4\epsilon_1 l_1,\epsilon_2 l_2\xrightarrow{\gamma}p^5\epsilon_1 l_1\xrightarrow{\gamma}p^5\epsilon l$
	(b) $p^6\xrightarrow{V}p^4\epsilon_1 l_1\epsilon_2 l_2\xrightarrow{\gamma}p^5\epsilon l\epsilon_2 l_2\xrightarrow{\gamma}p^5\epsilon l$
	(c) $p^6\xrightarrow{V}p^4\epsilon l\epsilon_1 l_1\xrightarrow{\gamma}p^4\epsilon l\epsilon_2 l_2\xrightarrow{\gamma}p^5\epsilon l$
(4) Intermediate-state shake-up interactions	$p^6\xrightarrow{\gamma}p^5\epsilon_1 l_1\xrightarrow{V}p^4\epsilon l\epsilon_1 l_1\xrightarrow{\gamma}p^5\epsilon l$
(5) Intermediate-state electron scattering interactions	$p^6\xrightarrow{\gamma}p^5\epsilon_1 l_1\xrightarrow{V}p^4\epsilon l\epsilon_2 l_2\xrightarrow{\gamma}p^5\epsilon l$
(6) Final-state electron scattering interactions	(a) $p^6\xrightarrow{\gamma}p^5\epsilon_1 l_1\xrightarrow{\gamma}p^4\epsilon_1 l_1\epsilon_2 l_2\xrightarrow{V}p^5\epsilon l$
	(b) $p^6\xrightarrow{\gamma}p^5\epsilon_2 l_2\xrightarrow{\gamma}p^4\epsilon_1 l_1\epsilon_2 l_2\xrightarrow{V}p^5\epsilon l$

[a]The symbols γ and V indicate that the transitions indicated are induced, respectively, by the electric dipole operator and the perturbation operator, $V\equiv\sum_{i>j}r_{ij}^{-1}-V_{\rm HF}$, where $\sum_{i>j}r_{ij}^{-1}$ is the Coulomb interaction operator and $V_{\rm HF}$ is the appropriate Hartree-Fock nonlocal potential.

cesses of first order in V are distinguished by whether they involve ground-state, intermediate-state, or final-state correlation effects, as in the ordering of terms for the amplitudes in Eq. (7). In the subsections which follow, we illustrate our *ad hoc* variational procedures for a few of the key processes listed in Table I which contribute to the two-photon transition amplitudes. We note that the description of correlation effects to first order in V in Eq. (7) has been made for simplicity. As described below, we have in actuality treated many effects to higher order. Specifically, intermediate-state interchannel interactions are treated to infinite order, and certain dipole amplitudes have been replaced by effective dipole amplitudes.

B. Lowest-order and intermediate-state interchannel effects

It is convenient to treat processes (1a) and (2) in Table I simultaneously as well as to infinite order in V by defining a projection PHP of the exact Hamiltonian H onto the space of all states having a single electron excited from the outer p^6 subshell, where P is a projection operator defined by

$$P \equiv \sum_{l'} \int d\epsilon' |np^5\epsilon' l'(^1P)\rangle\langle np^5\epsilon' l'(^1P)| \ . \tag{9}$$

Here the states all have ^1P symmetry, as is appropriate for electric dipole excitations from a ^1S initial state. Thus the exact two-photon transition amplitude in Eq. (1) may be approximated by

$$T^{(2)}_{i\to f}(\text{processes (1a)+(2)}) = \langle f_{\rm HF}|DP(E_i^{\rm HF}+\omega-PHP)^{-1}PD|i_{\rm HF}\rangle \ , \tag{10}$$

where the HF initial and final states are defined in Eqs. (4) and (5). In obtaining Eq. (10), we have ignored all matrix elements belonging to PHQ or QHP, where $Q \equiv 1-P$. We evaluate Eq. (10) using variationally stable techniques.[33,34] Thus we write

$$T^{(2)}_{i\to f}(\text{processes (1a)+(2)}) = \langle f_{\rm HF}|D|\Lambda_i\rangle + \langle \Lambda_f|D|i_{\rm HF}\rangle - \langle \Lambda_f|(E_i^{\rm HF}+\omega-PHP)|\Lambda_i\rangle \ , \tag{11}$$

where the states $\langle \Lambda_f|$ and $|\Lambda_i\rangle$ are defined formally by[28,29]

$$|\Lambda_i\rangle \equiv P(E_i^{\rm HF}+\omega-PHP)^{-1}PD|i_{\rm HF}\rangle \ , \tag{12}$$

$$\langle \Lambda_f| \equiv \langle f_{\rm HF}|DP(E_i^{\rm HF}+\omega-PHP)^{-1}P \ . \tag{13}$$

Because of the projection operator P, we may write Λ_i and Λ_f explicitly in terms of the unknown one-electron orbitals $\lambda^i_{l_2}$ and $\lambda^f_{l_1}$, as follows:

$$|\Lambda_i\rangle \equiv \sum_{l_2} |np^5\lambda^i_{l_2}(^1P)\rangle \ , \tag{14}$$

$$\langle \Lambda_f| \equiv \sum_{l_1} \langle np^5\lambda^f_{l_1}(^1P)| \ . \tag{15}$$

For electric dipole processes of course, l_1 and l_2 are restricted to the values 0 and 2, which we indicate by the subscripts s and d below. Substituting Eqs. (14) and (15) into Eq. (11) and carrying out all angular integrations gives

$$T^{(2)}_{i\to f}(\text{processes (1a)+(2)}) = a_d b_d[\langle \epsilon l|r|\lambda^i_d\rangle + \langle \lambda^f_d|r|np\rangle] + a_s b_s[\langle \epsilon l|r|\lambda^i_s\rangle + \langle \lambda^f_s|r|np\rangle] - (a_d\langle \lambda^f_d|, a_s\langle \lambda^f_s|) \begin{pmatrix} \epsilon_{np}+\omega-h_d^{\,^1P} & -v_{ds} \\ -v_{sd} & \epsilon_{np}+\omega-h_s^{\,^1P} \end{pmatrix} \begin{pmatrix} b_d|\lambda^i_d\rangle \\ b_s|\lambda^i_s\rangle \end{pmatrix} \ . \tag{16}$$

In Eq. (16), $a_d(l,L)$, $a_s(l,L)$, b_d, and b_s are angular factors for the electric dipole transitions from the initial state to the intermediate state (b_d and b_s) and from the intermediate state to the final state (a_d and a_s) and are given in the Appendix; $h_l^{\,^1P}$ is the LS-dependent one-electron radial HF Hamiltonian[37,38] for $LS = {}^1P$; ϵl and np denote the one-electron HF radial wave functions for the active electron in the initial and final states; ϵ_{np} is the HF energy for the initial one-electron orbital np; and v_{ds} and v_{sd} are the one-electron off-diagonal interchannel interaction operators, which are also given in the Appendix. In obtaining Eq. (16) we have used the fact that

$$PHP = PH_{\rm HF}P + PVP \ , \tag{17}$$

as well as the fact that $PH_{\rm HF}P$ has only diagonal matrix elements and PVP has only off-diagonal matrix elements.

Equation (16) is solved by expanding each λ_l in a Slater orbital basis,

$$\lambda_l(r) \equiv \sum_n \alpha_n f_n(l,\beta;r) \ , \tag{18}$$

where

$$f_n(l,\beta;r) \equiv N_n r^{l+n} e^{-\beta r} \ , \tag{19}$$

and where α_n are the expansion coefficients, N_n is a normalization factor, and β may be real or complex and is chosen intuitively for each specific calculation. The coefficients α_n are obtained by enforcing the variational stability condition for the amplitude in Eq. (16).[34,39]

It is straightforward to generalize the procedure described in this section to treat also interchannel interactions among states having single electrons excited out of

inner subshells. Near the single-photon ionization threshold and above, these interactions may produce additional resonances. In this work, however, we have only included the contributions of excitations from the ns^2 inner shells to the two-photon transition amplitude in lowest-order (HF) approximation, corresponding to process (1b) in Table I. Besides interchannel interactions, there are other important intermediate-state electron correlations. Since these involve doubly excited intermediate states, we have treated them perturbatively. We describe our treatment of some of these interactions later.

C. Ground-state correlations

Processes (3a) and (3b) in Table I both involve a double excitation out of the np^6 ground-state configuration followed by two successive photon absorption processes, one of which further excites one of the doubly excited electrons and one of which deexcites the other electron back to the final core configuration, np^5. Processes (3a) and (3b) differ only in the time ordering of the photon absorption processes. Specifically, process (3a) represents the third-order amplitude

$$T(\text{process (3a)})=\int d\epsilon_1 \int d\epsilon_2 \sum_{l_1,l_2}\sum_{\tilde{L},\tilde{S}}\sum_{\bar{L},\bar{S}} \langle np^5\epsilon l(^1L)|D|np^5\epsilon_1 l_1(^1P)\rangle \frac{1}{\epsilon_{np}+\omega-\epsilon_1} \times\langle np^5\epsilon_1 l_1(^1P)|D|np^4(\tilde{L}\tilde{S})\epsilon_2 l_2(\bar{L}\bar{S})\epsilon_1 l_1(^1S)\rangle \times\frac{1}{2\epsilon_{np}-\epsilon_1-\epsilon_2}\langle np^4(\tilde{L}\tilde{S})\epsilon_2 l_2(\bar{L}\bar{S})\epsilon_1 l_1(^1S)|V|np^6(^1S)\rangle , \tag{20}$$

and process (3b) represents the third-order amplitude,

$$T(\text{process (3b)})=\int d\epsilon_1 \int d\epsilon_2 \sum_{l_1,l_2}\sum_{\tilde{L},\tilde{S}}\sum_{\bar{L},\bar{S}} \langle np^5\epsilon l(^1L)|D|np^4(\tilde{L}\tilde{S})\epsilon_2 l_2(\bar{L}\bar{S})\epsilon l(^1P)\rangle \times\frac{1}{2\epsilon_{np}+\omega-\epsilon_2-\epsilon} \times\langle np^4(\tilde{L}\tilde{S})\epsilon_2 l_2(\bar{L}\bar{S})\epsilon l(^1P)|D|np^4(\tilde{L}\tilde{S})\epsilon_2 l_2(\bar{L}\bar{S})\epsilon_1 l_1(^1S)\rangle \times\frac{1}{2\epsilon_{np}-\epsilon_1-\epsilon_2}\langle np^4(\tilde{L}\tilde{S})\epsilon_2 l_2(\bar{L}\bar{S})\epsilon_1 l_1(^1S)|V|np^6(^1S)\rangle . \tag{21}$$

The two amplitudes in Eqs. (20) and (21) have the same angular and radial factors; they differ only in the energy denominators. Using the fact that the photoelectron energy in the final state ϵ is equal to $2\omega+\epsilon_{np}$, the two amplitudes may be combined to obtain

$$T(\text{process (3a)})+T(\text{process (3b)}) =\sum_k \sum_{l_1,l_2} A(k,l_1,l_2,l,L)\rho^k(l_1,l_2) , \tag{22}$$

where A is the angular factor, given in the Appendix, and where the radial factor ρ is defined by

$$\rho^k(l_1,l_2)\equiv\int d\epsilon_1\int d\epsilon_2(\epsilon l|r|\epsilon_1 l_1)\frac{1}{\epsilon_{np}+\omega-\epsilon_1} \times(np|r|\epsilon_2 l_2)\frac{1}{\epsilon_{np}-\omega-\epsilon_2} \times R^k(\epsilon_2 l_2,\epsilon_1 l_1;np,np) . \tag{23}$$

In Eq. (23), the Slater integral R^k is defined by

$$R^k(\epsilon_2 l_2,\epsilon_1 l_1;np,np)\equiv\int_0^\infty dr\, u_{\epsilon_1 l_1}(r)u_{np}(r)y_k(\epsilon_2 l_2,np;r) , \tag{24}$$

where the $u_{nl}(r)$ are the one-electron radial wave functions, and where the function y_k is defined by

$$y_k(a,b;r)\equiv r^{-(k+1)}\int_0^r t^k u_a(t)u_b(t)dt +r^k\int_r^\infty t^{-(k+1)}u_a(t)u_b(t)dt . \tag{25}$$

Also, the length form electric dipole radial integrals are defined by

$$(a|r|b)\equiv\int_0^\infty dr\, u_a(r)ru_b(r) . \tag{26}$$

It is the radial function $\rho^k(l_1,l_2)$ which we wish to evaluate by variationally stable, implicit summation techniques. Using the HF ^1P one-electron radial Hamiltonian for each of the two intermediate-state excited electrons, we may write $\rho^k(l_1,l_2)$ as follows:

$$\rho^k(l_1,l_2)=R^k(\lambda_{l_2}^{np},\lambda_{l_1}^{\epsilon l};np,np) , \tag{27}$$

where

$$\langle\lambda_{l_2}^{np}|\equiv\langle np|r[\epsilon_{np}-\omega-h_{l_2}^{^1P}(r)]^{-1} \tag{28}$$

and where

$$\langle\lambda_{l_1}^{\epsilon l}|\equiv\langle\epsilon l|r[\epsilon_{np}+\omega-h_{l_1}^{^1P}(r)]^{-1} . \tag{29}$$

The use of the HF ^1P radial Hamiltonian for each of the excited electrons is a common approximation, which is employed, e.g., in random-phase approximation (RPA) calculations. We evaluate Eq. (27) in two steps, each of which we describe now in turn.

1. Evaluation of $\lambda_{l_2}^{np}(r)$

Note that $\lambda_{l_2}^{np}(r)$, defined in Eq. (28), satisfies an inhomogeneous equation for which the "energy" is $\epsilon_{np}-\omega$, which is more negative than the np ground-state orbital energy. Since such a function should be very well localized, we have represented $\lambda_{l_2}^{np}(r)$ as an explicit expansion in N Slater orbitals, as in Eq. (18), where the coefficients α_n of the expansion may be obtained as the solutions of the following set of linear, inhomogeneous equations:[39]

$$\sum_{n=1}^{N} \alpha_n \langle f_n | \epsilon_{np}-\omega-h_{l_2}^{1P}(r) | f_m \rangle = \langle np | r | f_m \rangle \ , \quad (30)$$

where $1 \le m \le N$.

2. Evaluation of $\rho^k(l_1,l_2)$

With $\lambda_{l_2}^{np}$ known, there is only a single summation required to evaluate $\rho^k(l_1,l_2)$ in Eq. (27), namely, that defined implicitly by the function $\lambda_{l_1}^{\epsilon l}$ [cf. Eq. (29)]. Rather than calculate $\lambda_{l_1}^{\epsilon l}$ explicitly for substitution in Eq. (27), we use instead variationally stable techniques to evaluate $\rho^k(l_1l_2)$ directly. Thus we write the amplitude $\rho^k(l_1,l_2)$ in Eq. (27) in the following form, using Eqs. (24) and (29):

$$\rho^k(l_1,l_2)=\langle \epsilon l | r [\epsilon_{np}+\omega-h_{l_1}^{1P}(r)]^{-1} y_k(\lambda_{l_2}^{np},np;r) | np \rangle \ . \quad (31)$$

Defining the implicit function,

$$|\bar{\lambda}_{l_1,l_2}^{np}\rangle \equiv [\epsilon_{np}+\omega-h_{l_1}(r)]^{-1} y_k(\lambda_{l_2}^{np},np;r)|np\rangle \ , \quad (32)$$

Eq. (31) may be written in a variationally stable form[34] as

$$\rho^k(l_1,l_2)=\langle \lambda_{l_1}^{\epsilon l} | y_k(\lambda_{l_2}^{np},np;r)|np\rangle + \langle \epsilon l | r | \bar{\lambda}_{l_1,l_2}^{np}\rangle - \langle \lambda_{l_1}^{\epsilon l} | [\epsilon_{np}+\omega-h_{l_1}^{1P}(r)] | \bar{\lambda}_{l_1,l_2}^{np}\rangle \ , \quad (33)$$

where $\lambda_{l_1}^{\epsilon l}$ has been defined in Eq. (29). Equation (33) is evaluated numerically by representing $\lambda_{l_1}^{\epsilon l}$ and $\bar{\lambda}_{l_1,l_2}^{np}$ as expansions in Slater orbitals and evaluating the coefficients by enforcing the variational stability condition[34,39] on Eq. (33).

3. Process (3c)

The ground-state correlation process (3c) in Table I involves an initial double excitation followed by deexcitation of one of the excited electrons by the two absorbed photons back to the initial state. For this deexcitation part of the process the other excited electron is a spectator. Since one of the excited electrons starts and ends in the bound np orbital, this process is easily treated by variationally stable procedures similar to those described already.

D. Other intermediate-state interactions

When the first photon absorption produces a singly excited intermediate state, it is possible for either the core or the excited electron to excite another electron out of the core by means of the perturbation V. These two processes are described schematically by (4) and (5) in Table I. We discuss each in turn.

1. Intermediate-state shake-up interactions

Process (4) in Table I has the following transition amplitude:

$$T_{i\to f}^{(2)}(\text{process (4)}) = \sum_{\tilde{L},\tilde{S}} \sum_{\bar{L},\bar{S}} \sum_{l_1} \int d\epsilon_1 \langle np^5 \epsilon l(^1L)|D|np^4(\tilde{L}\tilde{S})\epsilon l(\bar{L}\bar{S})\epsilon_1 l_1(^1P)\rangle \frac{1}{\epsilon_{np}-\omega-\epsilon_1} \times \langle np^4(\tilde{L}\tilde{S})\epsilon l(\bar{L}\bar{S})\epsilon_1 l_1(^1P)|V|np^5\epsilon_1 l_1(^1P)\rangle \frac{1}{\epsilon_{np}+\omega-\epsilon_1} \times \langle np^5\epsilon_1 l_1(^1P)|D|np^6(^1S)\rangle \ . \quad (34)$$

Carrying out the angular integrations, one obtains

$$T_{i\to f}^{(2)}(\text{process (4)}) = \sum_{k,l_1} B(k,l_1,l,L) R^k(np,\epsilon l,np,np)\tau(l_1) \ , \quad (35)$$

where $B(k,l_1,l,L)$ is the angular factor, given in the Appendix, and $\tau(l_1)$ is defined by

$$\tau(l_1) \equiv \int d\epsilon_1 \langle np|r|\epsilon_1 l_1\rangle \frac{1}{(\epsilon_{np}-\omega-\epsilon_1)(\epsilon_{np}+\omega-\epsilon_1)} \times \langle \epsilon_1 l_1 | r | np\rangle \ . \quad (36)$$

Equation (36) is troublesome in its current form because the two energy denominators depend on the same variable ϵ_1. They may be uncoupled, however, using orthonormality of the continuum orbitals,

$$\langle \epsilon_1 l_1 | \epsilon_2 l_1 \rangle = \delta(\epsilon_1-\epsilon_2) \ . \quad (37)$$

Representing, then, the corresponding two Green's functions in operator form, i.e.,

$$\int d\epsilon \frac{|\epsilon l_1\rangle\langle \epsilon l_1|}{\epsilon_{np}\pm\omega-\epsilon} \equiv \frac{1}{\epsilon_{np}\pm\omega-h_{l_1}^{1P}} \ , \quad (38)$$

we may write $\tau(l_1)$ as

$$\tau(l_1) \equiv \langle np | r (\epsilon_{np}-\omega-h_{l_1}^{1P})^{-1}(\epsilon_{np}+\omega-h_{l_1}^{1P})^{-1} r | np\rangle \ . \quad (39)$$

Finally, introducing $\langle \lambda_{l_1}^{np}|$, which is defined in Eq. (28) and calculated as in Sec. II C 1 above, we get

$$\tau(l_1)\equiv\langle \lambda_{l_1}^{np}|(\epsilon_{np}+\omega-h_{l_1}^{1P})^{-1}r|np\rangle \ . \tag{40}$$

Equation (40) is then evaluated using variationally stable procedures similar to those already described.

2. *Intermediate-state electron scattering interactions*

These are described schematically by process (5) in Table I. Unlike the shake-up process described above, the two energy denominators are uncoupled in the sense that they contain kinetic energies of two different excited electrons. Use once again of λ_l^{np}, defined in Eq. (28) and calculated as in Sec. II C 1 above, reduces the radial amplitude to a form which is easily evaluated by variationally stable procedures already described.

E. Final-state electron scattering interactions

This interaction, described schematically by process (6) in Table I, has a very important effect on the two-photon transition amplitudes, as has been described elsewhere (Refs. 10, 12, 13, 20, and 21). In all of these previous works, however, this interaction is calculated in the RPA. Instead, we evaluate the angular factor for this interaction exactly, taking full account of the Pauli exclusion principle; the radial integrals are then evaluated by the method described below.

The transition amplitude for process (6a) is

$$\begin{aligned}T_{i\to f}^{(2)}(\text{process (6a)})=\sum_{\bar L,\tilde S}\sum_{\bar L,\bar S}\sum_{l_1 l_2}\int d\epsilon_1\int d\epsilon_2\langle np^5\epsilon l(^1L)|V|np^4(\bar L\tilde S)\epsilon_1 l_1(\bar L\bar S)\epsilon_2 l_2(^1L)\rangle\\ \times\frac{1}{2\epsilon_{np}+2\omega-\epsilon_1-\epsilon_2}\langle np^4(\bar L\tilde S)\epsilon_1 l_1(\bar L\bar S)\epsilon_2 l_2(^1L)|D|np^5\epsilon_1 l_1(^1P)\rangle\\ \times\frac{1}{\epsilon_{np}+\omega-\epsilon_1}\langle np^5\epsilon_1 l_1(^1P)|D|np^6(^1S)\rangle \ .\end{aligned} \tag{41}$$

A similar expression applies for process (6b), in which the time ordering of the two electric dipole excitations is reversed. Combining the amplitudes for processes (6a) and (6b) and evaluating all angular factors exactly gives the following result:

$$T_{i\to f}^{(2)}(\text{processes (6a)+(6b)})=\sum_{k,l_1,l_2}C(k,l_1,l_2,l,L)\chi(k,l_1,l_2) \ , \tag{42}$$

where the angular factor $C(k,l_1,l_2,l,L)$ is given in the Appendix and where

$$\begin{aligned}\chi(k,l_1,l_2)\equiv\int d\epsilon_1\int d\epsilon_2 R^k(np,\epsilon l;\epsilon_2 l_2,\epsilon_1 l_1)\\ \times\frac{1}{\epsilon_{np}+\omega-\epsilon_2}\langle\epsilon_2 l_2|r|np\rangle\\ \times\frac{1}{\epsilon_{np}+\omega-\epsilon_1}\langle\epsilon_1 l_1|r|np\rangle \ .\end{aligned} \tag{43}$$

Define now the following implicit functions:

$$\langle\lambda_1(np,\epsilon l,l_1,l_2)|\equiv\int d\epsilon_1 R^k(np,\epsilon l;\lambda_{l_2}^{np},\epsilon_1 l_1)(\epsilon_{np}+\omega-\epsilon_1)^{-1}\langle\epsilon_1 l_1| \ , \tag{44}$$

$$\langle\lambda_2(np,\epsilon l,l_1,l_2)|\equiv\int d\epsilon_2 R^k(np,\epsilon l;\epsilon_2 l_2,\lambda_{l_1}^{np})(\epsilon_{np}+\omega-\epsilon_2)^{-1}\langle\epsilon_2 l_2| \ , \tag{45}$$

where $\lambda_{l_1}^{np}$ and $\lambda_{l_2}^{np}$ are defined as in Eq. (29). We may then write χ in the following variationally stable form:

$$\begin{aligned}\chi(k,l_1,l_2)=R^k(np,\epsilon l;\lambda_{l_2}^{np},\lambda_{l_1}^{np})+\langle\lambda_1|r|np\rangle\\ -\langle\lambda_1|\epsilon_{np}+\omega-h_{l_1}^{1P}|\lambda_{l_1}^{np}\rangle+\langle\lambda_2|r|np\rangle\\ -\langle\lambda_2|\epsilon_{np}+\omega-h_{l_2}^{1P}|\lambda_{l_2}^{np}\rangle \ .\end{aligned} \tag{46}$$

The implicit functions λ_1, λ_2, $\lambda_{l_1}^{np}$, and $\lambda_{l_2}^{np}$ in Eq. (46) are each expanded in a Slater orbital basis and the coefficients of these expansions are obtained, as usual, by requiring Eq. (46) to be variationally stable.[34,39]

F. Higher-order interactions

It is convenient to include effects of ground-state correlations and interchannel interactions in evaluating the third-order amplitudes for processes (4)–(6). Each of these processes starts as an electric dipole excitation to a singly excited intermediate state. Effects of ground-state and interchannel interactions may be included by replacing the initial electric dipole radial operator by an effective electric dipole radial operator. Such procedures are common in many-body theory, and have been employed previously for two-photon processes.[13]

Specifically, to include ground-state correlation effects to first order in each of these processes we may simply make the following replacement:

$$\langle\epsilon l_1|r|np\rangle\to\langle\epsilon l_1|r|np\rangle+\sum_{k,l_2}d(k,l_1,l_2)R^k(\lambda_{l_2}^{np},\epsilon l_1;np,np) \ , \tag{47}$$

where R^k is defined by Eq. (24), $\lambda_{l_2}^{np}$ is defined by Eq. (28), and $d(k,l_1,l_2)$ is an angular factor given in the Appendix. In a similar way, interchannel interactions can be

taken into account to infinite order by making the replacement

$$(\epsilon_{np}+\omega-h_l^{1P})^{-1}r|np\rangle \rightarrow |\lambda_l^i\rangle \ , \tag{48}$$

where the implicit function $|\lambda_l^i\rangle$ is obtained from solving Eq. (16).

III. TWO-PHOTON IONIZATION CROSS SECTIONS FOR Ar

We are concerned with the calculation of the cross sections for each of the following transitions:

$$\text{Ar } 3p^6(^1S)+2\gamma \rightarrow \text{Ar}^+3p^5(^2P)\epsilon p(^1S) \tag{49a}$$

$$\rightarrow \text{Ar}^+3p^5(^2P)\epsilon p(^1D) \tag{49b}$$

$$\rightarrow \text{Ar}^+3p^5(^2P)\epsilon f(^1D) \ . \tag{49c}$$

We discuss first some numerical details of our calculations and then present our cross-section results for each of these three channels as well as for the total cross sections.

A. Numerical details

We have used the Roothaan-HF wave functions tabulated by Clementi and Roetti[40] to describe the Ar $3p^6(^1S)$ single-configuration ground state. These were then used as our frozen-core orbitals in intermediate and final states. The final-state wave function for the photoelectron in each of the configurations on the right in Eq. (49) was calculated in the appropriate LS-dependent HF potential.[37,38] Orthogonality of the continuum p-electron wave functions to the bound $2p$ and $3p$ wave functions was assured by calculating both the bound and continuum orbitals in the same Hermitian potential, as described in Refs. 41–45. Each of our continuum wave functions was energy normalized at large radial distances:

$$\psi_l(k,r)=\left[\frac{2}{\pi\zeta(l,k,r)}\right]^{1/2}\sin[\theta(l,k,r)+\delta] \ , \tag{50a}$$

where

$$\theta(l,k,r) \underset{r\rightarrow\infty}{\sim} kr-\tfrac{1}{2}\pi l+k^{-1}\ln(2kr) + \arg\Gamma(l+1-i/k) \ , \tag{50b}$$

$$\zeta(l,k,r) \underset{r\rightarrow\infty}{\sim} k \ . \tag{50c}$$

In Eq. (50), $k^2/2$ is the kinetic energy of the photoelectron and δ is the phase shift with respect to a Coulomb wave. The phase function $\theta(l,k,r)$ and the amplitude function $\zeta(l,k,r)$ are calculated at large but finite r using the procedure of Burgess.[46] In our calculations we have ignored the final-state interchannel coupling between the $f(^1D)$ and $p(^1D)$ channels.

In calculating the various contributions to the total two-photon transition amplitude, we have employed Slater orbital expansions of the type shown in Eq. (18), as discussed in Sec. II. Typically we employed 40–50 Slater orbitals for each such expansion. For low-n values [cf. Eq. (18)] several different exponents β [cf. Eq. (19)] were used, while for higher-n values only a single β value was used. Our calculations were carried out using double precision arithmetic (120 bit) on a CDC 835 computer. Generally we were able to obtain convergence of our amplitudes to better than 1 part in 10^3.

Accurate depiction of the prominent resonance structure in the two-photon ionization cross section of argon requires detailed consideration of the binding energies employed. For all processes described in Sec. II in which the intermediate state is singly excited and characterized by a one-electron Green's function of the form $(\epsilon_{3p}+\omega-h_l^{LS})^{-1}$, we have replaced the HF $3p$ orbital binding energy of 16.08 eV by the experimental[47] $3p$ subshell binding energy of 15.76 eV. Furthermore, in calculating our final-state wave functions, the kinetic energy of the photoelectron is related to the photon energy by $k^2/2=2\omega-15.76$ eV. Because of our implicit summation over intermediate states, it is not possible to shift the positions of intermediate-state resonances into exact agreement with experiment, as would be possible using an explicit summation over intermediate states. Nevertheless, our use of the experimental single ionization binding energy wherever feasible improves our predicted resonance positions significantly.

The binding energies employed in evaluating the transition amplitude for process (6) in Table I require special consideration, as has been noted in similar calculations for xenon.[48] This process has been discussed in detail in Sec. II E above in the approximation that the perturbation operator V is included only to first order. This approximation results in Eq. (43) for the radial part of the transition amplitude, which contains two single-particle Green's functions, $(\epsilon_{3p}+\omega-h_l^{1P})^{-1}$. Because of this, double excitation resonances as well as the double ionization threshold occur much lower in energy than is observed experimentally. Hence their effect on the predictions for the two-photon, single ionization cross section and, in particular, on the widths of the single excitation resonances, is exaggerated. We have corrected this difficulty in the following approximate, *ad hoc* way. Rather than replace both of the HF ϵ_{3p} energies in Eq. (43) by the negative of the experimental *single* ionization binding energy, $\epsilon_{3p}^{\text{expt}}$, we have replaced one of them by the negative of one-half the experimental[48] double ionization binding energy, $\epsilon_{3p^2}^{\text{expt}}$, which equals 43.4 eV. Thus, in Eq. (43) we make the replacement

$$\begin{aligned}(\epsilon_{3p}+\omega-\epsilon_2)^{-1}(\epsilon_{3p}+\omega-\epsilon_1)^{-1}=0.5[&(0.5\epsilon_{3p^2}^{\text{expt}}+\omega-\epsilon_2)^{-1}(\epsilon_{3p}^{\text{expt}}+\omega-\epsilon_1)^{-1}\\ &+(\epsilon_{3p}^{\text{expt}}+\omega-\epsilon_2)^{-1}(0.5\epsilon_{3p^2}^{\text{expt}}+\omega-\epsilon_1)^{-1}]\\ =&(\epsilon_{3p^2}^{\text{expt}}+2\omega-2\epsilon_2)^{-1}(\epsilon_{3p}^{\text{expt}}+\omega-\epsilon_1)^{-1}+(\epsilon_{3p}^{\text{expt}}+\omega-\epsilon_2)^{-1}(\epsilon_{3p^2}^{\text{expt}}+2\omega-2\epsilon_1)^{-1} \ .\end{aligned} \tag{51}$$

In this way, the correct single and double ionization threshold binding energies are approximately included in our calculations, thereby reducing somewhat the effect of final-state electron scattering interactions on the two-photon cross section and giving a much more reliable description of the lowest intermediate state, single-excitation resonances.

B. Results for the two-photon ionization cross sections

In lowest-order perturbation theory the N-photon ionization rate W is given by[49]

$$W=\sigma_N I^N . \tag{52}$$

Here σ_N is a generalized N-photon cross section dependent only on properties of the atomic or ionic target and on the polarization of the incident light and I is the intensity of the laser field. W is usually measured in units of ions/sec, σ_N in units of $\mathrm{cm}^{2N}\mathrm{sec}^{N-1}$, and I in units of photons/(cm^2 sec). For two-photon ionization, the generalized cross section in atomic units (i.e., $e=\hbar=m=1$) is

$$\sigma_2^q=\frac{8\pi^3\omega^2}{c^2}|T|^2 f_q \quad \text{(a.u.)} . \tag{53}$$

Here ω is the photon energy, c is the speed of light, T is the reduced transition amplitude discussed in Sec. II, and f_q is a geometrical factor dependent on the polarization q of the photons and on the final-state term level. Table II gives the values of f_q for the cases of interest in this paper. Conversion of Eq. (53) to the usual units cm^4 sec requires the conversion of the dimension L^4T from a.u. to cgs units,

$$L^4T \text{ (a.u.)}=1.8967\times10^{-50}\ \mathrm{cm}^4\,\mathrm{sec} . \tag{54}$$

We present our results for the generalized two-photon cross section for each of the three transitions in Eq. (49) in the case of linearly polarized photons in Figs. 1–3. In Fig. 1(a) we see that in lowest order, i.e., HF approximation, the dipole length and velocity results for the $p(^1S)$ final-state channel differ by more than a factor of 3. Furthermore, the width of the Ar $3p^54s(^1P)$ intermediate-state resonance in the length results is more than an order of magnitude larger than in the velocity results. Inclusion of ground-state correlations and intermediate-state interchannel interactions [cf. processes (2) and (3) in Table I] hardly diminishes the discrepancies between the length and velocity results. In Fig. 1(b) we see that inclusion of intermediate-state and final-state electron scattering interactions [cf. processes (5) and (6) in Table I] causes a dramatic lowering of the velocity results but only a modest lowering of the length results in the region below the $4s$ resonance. Inclusion of intermediate-state shake-up interactions [cf. process (4) in Table I), however, lowers further the length results and raises the velocity results into near agreement with the length results. Furthermore, it reduces the width of the length results for the $4s$ resonances dramatically, bringing them into reasonable agreement with the velocity results. For clarity, we have not presented all curves in the region above 14 eV, where near 14 eV there are the Ar $3p^53d(^1P)$ and Ar $3p^55s(^1P)$ intermediate-state resonances (unresolved in Fig. 1) and near 15 eV there are the Ar $3p^54d(^1P)$ and Ar $3p^56s(^1P)$ intermediate-state resonances (also unresolved in Fig. 1). We see, however, that for these higher-energy resonances also electron correlations have narrowed the initial HF length results considerably.

TABLE II. Values for f_q [cf. Eq. (53)] for linearly polarized ($q=0$) and circularly polarized ($q=\pm1$) photons.

q	Final-state term level	f_q
0	^1S	$\frac{1}{9}$
0	^1D	$\frac{2}{45}$
±1	^1S	0
±1	^1D	$\frac{1}{15}$

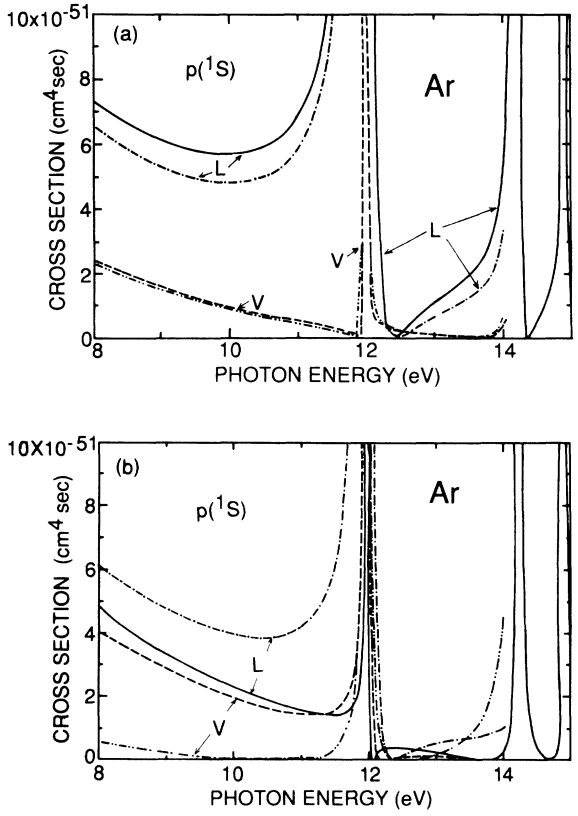

FIG. 1. Generalized two-photon cross section for the transition Ar $3p^6(^1S)+2\gamma\rightarrow Ar^+3p^5\epsilon p(^1S)$ for photon energies below the single ionization threshold for the case of linearly polarized light. L and V indicate electric dipole length and velocity results, respectively. (a) Solid and dashed curves, HF results. Dash-dotted and dash-double-dotted curves, results including processes (1)–(3) in Table I. (b) Dash-dotted and dash-double-dotted curves, results including processes (1)–(3), (5), and (6) in Table I. Solid and dashed curves, results including all processes listed in Table I.

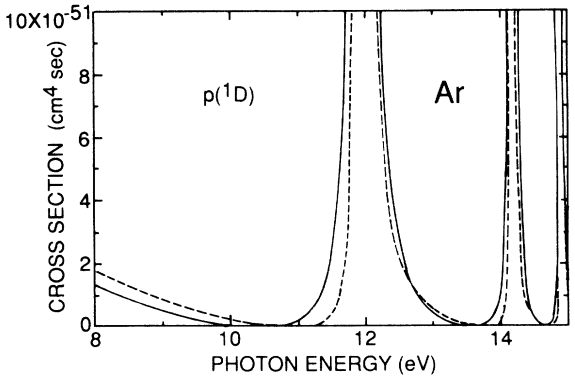

FIG. 2. Generalized two-photon cross section for the transition Ar $3p^6+2\gamma \rightarrow Ar^+3p^5\epsilon p(^1D)$ for photon energies below the single ionization threshold for the case of linearly polarized light. Dashed curve, HF length results. Solid curve, length results including all processes listed in Table I.

In Fig. 2, we see that our lowest-order, i.e., HF approximation, dipole length results for the $p(^1D)$ final-state channel are quite close to our "fully correlated" dipole length results, which include all processes listed in Table I. Such is not the case for the $f(^1D)$ channel, as shown in Fig. 3. Here the HF dipole length results (dash-dot curve) are the largest (on average) and do not indicate any of the Ar $3p^5ns(^1P)$ intermediate-state resonances, which only appear when interchannel interactions are introduced. This is seen in the dashed curve, which includes both ground-state and intermediate-state interchannel interactions. Inclusion of the remaining interactions in Table I, in particular, the final-state electron scattering interactions, results in a change in the sign of the resonance profile parameter,[50] as shown by a comparison of the solid and dashed curves.

Figures 4 and 5 show our results for the total two-photon ionization cross sections in the cases of linearly and circularly polarized light, respectively. As was the case for the $p(^1S)$ channel results shown in Fig. 1, the dipole length total cross-section results for linear polariza-

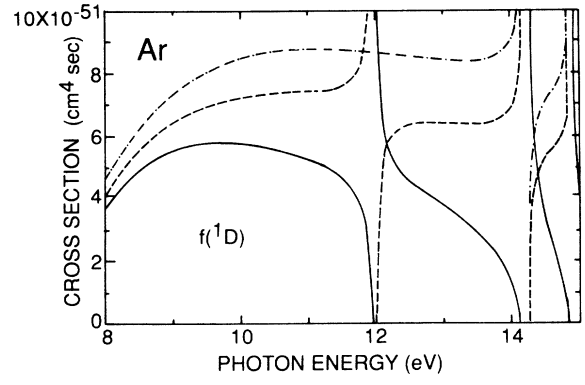

FIG. 3. Generalized two-photon cross section for the transition Ar $3p^6(^1S)+2\gamma \rightarrow Ar^+3p^5\epsilon f(^1D)$ for photon energies below the single ionization threshold for the case of linearly polarized light. Dash-dotted curve, HF length results. Dashed curve, length results including processes (1)–(3) in Table I. Solid curve, length results including all processes listed in Table I.

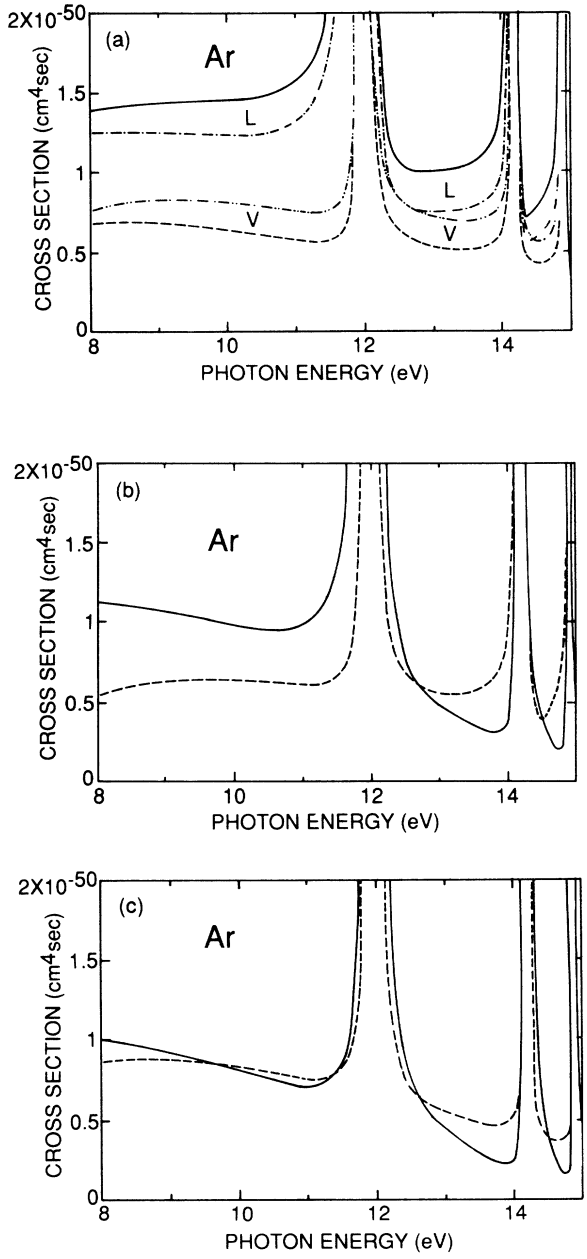

FIG. 4. Generalized two-photon total cross sections for the process Ar $3p^6(^1S)+2\gamma \rightarrow Ar^+3p^5(^2P)+e^-$ for the case of linearly polarized light. (a) Solid and dashed curves, dipole length and velocity results in HF approximation [cf. process (1) in Table I]. Dash-dotted and dash-double-dotted curves, dipole length and velocity results including ground-state and intermediate-state interchannel interactions [cf. processes (2) and (3)in Table I]. (b) Solid and dashed curves, dipole length and velocity results including, in addition, electron scattering interactions [cf. processes (5) and (6) in Table I]. (c) Solid and dashed curves, dipole length and velocity results including all processes listed in Table I.

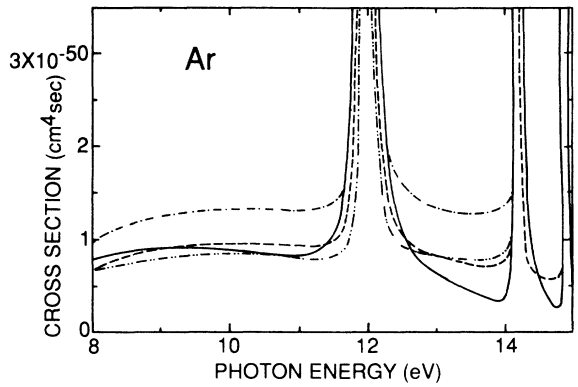

FIG. 5. Generalized two-photon total cross sections for the process Ar $3p^6(^1S)+2\gamma \rightarrow Ar^+3p^5(^2P)+e^-$ for the case of circularly polarized light. Dash-dotted and dash-double-dotted curves, lowest-order (HF) dipole length and velocity results. Solid and dashed curves, dipole length and velocity results including all processes listed in Table I.

tion, shown in Fig. 4, decrease steadily as the various electron correlation processes listed in Table I are included in the calculation. The dipole velocity results change less predictably. As shown in Fig. 4(c), our results including all of the electron correlations listed in Table I give good agreement of the dipole length and velocity results.

The results for the circular polarization cross sections, shown in Fig. 5, indicate a less dramatic change between the lowest-order HF level results and the results including all correlations listed in Table I. This is due primarily to the absence of any contribution of the $p(^1S)$ partial cross section to the total cross section for circularly polarized light. It is the $p(^1S)$ partial cross section in the case of linearly polarized light which exhibits the most dramatic influence of intermediate-state shake-up interactions, as discussed above.

C. Comparisons with other calculations

There have been three prior treatments of electron correlation effects on the two-photon ionization cross section of argon. Pindzola and Kelly,[6] in their many-body perturbation-theory (MBPT) calculation, treated the effects indicated by processes (1)–(3) in Table I for the $f(^1D)$ final-state channel; the $p(^1S)$ and $p(^1D)$ final-state channels were treated only in lowest order. Moccia, Rahman, and Rizzo[9] have calculated approximate random-phase approximation results, which employ relaxed core wave functions in the final state (as compared with our frozen-core wave functions) and which use continuum final-state wave functions calculated in a static exchange potential (as compared to our use of continuum HF wave functions calculated in the appropriate LS-dependent nonlocal potential[37,38]). An exact RPA calculation should in principle treat all processes listed in Table I except for the shake-up interactions [process (4)]. However, we emphasize hat the RPA angular factors for the scattering processes (5) and (6) in Table I ignore the Pauli principle; we have used instead the exact angular factors. Similarly, the transition matrix results of Starace and Jiang[12] also treat all processes listed in Table I except for the shake-up interactions [process (4)]. Another significant difference with our results is that they also used the RPA angular factors for the electron scattering interactions. Finally, we compare our results also with the central potential model results of McGuire,[8] which may be considered as an approximation to our lowest-order HF results.

In summary, then, in our calculation for two-photon ionization of argon we have included the influence of shake-up interactions, which we have found to be essential to bring into agreement length and velocity results for the $p(^1S)$ partial cross section, and hence also for the total cross section for linearly polarized light. It is interesting to note that Starace and Jiang[12] adduced indirect evidence that all three of the results in Refs. 6, 9,

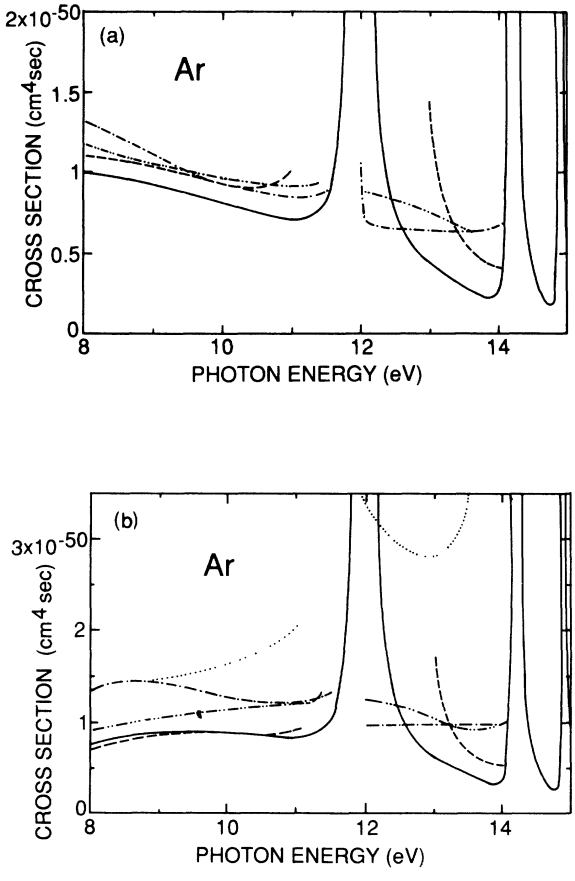

FIG. 6. Generalized two-photon total cross sections (dipole length) for the process Ar $3p^6(^1S)+2\gamma \rightarrow Ar^+3p^5(^2P)+e^-$. (a) Results for linearly polarized light. Solid curve, present results including all correlation processes listed in Table I. Dashed curve, Starace and Jiang (Ref. 12). Dash-dotted curve, Moccia, Rahman, and Rizzo (Ref. 9). Dash-double-dotted curve, Pindzola and Kelly (Ref. 6). (b) Results for circularly polarized light. Dotted curve, McGuire (Ref. 8). All other curves are as identified in (a).

and 12 differed significantly for the $p(^1S)$ partial cross section. We also have taken proper account of the Pauli principle in calculating the effect of electron scattering interactions [processes (5) and (6) in Table I].

We emphasize, however, that the near threshold two-photon ionization cross sections for argon are characterized by significant resonance structures. Differences in treating these resonances, therefore, also lead to significant differences in the predicted cross sections. Pindzola and Kelly[6] used experimental resonance energies; Moccia, Rahman, and Rizzo[9] used RPA resonance energies; Starace and Jiang[12] as well as this paper use HF level energies but experimental binding energies. Furthermore, in contrast to Starace and Jiang's[12] treatment of the final-state electron scattering interaction [process (6) in Table I], we have made an *ad hoc* attempt to introduce the experimental double ionization binding energy into our calculation, as discussed in Sec. III A above.

With these differences between the present and prior calculations in mind, we compare the results in Fig. 6. We make all comparisons for the dipole length results only, as we have demonstrated the greater reliability of these over the dipole velocity results. Figure 6(a) shows the total two-photon cross section for linearly polarized light and Fig. 6(b) shows the total two-photon cross section for circularly polarized light. As shown in Fig. 6(a), ours is the lowest result in the case of linearly polarized light, due almost entirely to our inclusion of the shake-up interactions [process (4) in Table I], which reduce the $p(^1S)$ partial cross section, and hence the total cross section, by $\approx 0.1\times10^{-50}$ cm^{4}sec [cf. Fig. 1(b)]. Without this interaction, we would essentially agree with the results of Starace and Jiang[12] near threshold. In contrast, as shown in Fig. 6(b), for circularly polarized light we essentially agree with the results of Starace and Jiang[12] near threshold. In both cases of incident light polarization, we have not attempted to make detailed comparisons of the various predictions for the intermediate-state resonance profiles. It is clear, however, that there are major differences both within the first resonance and between the first two resonances.

IV. TWO-PHOTON DETACHMENT CROSS SECTIONS FOR F^-

We are concerned with the calculation of the cross sections for each of the following transitions:

$$F^- \; 2p^6(^1S)+2\gamma \rightarrow F \; 2p^5(^2P)\epsilon p(^1S) \tag{55a}$$

$$\rightarrow F \; 2p^5(^2P)\epsilon p(^1D) \tag{55b}$$

$$\rightarrow F \; 2p^5(^2P)\epsilon f(^1D)\,. \tag{55c}$$

The numerical details of our calculations are essentially the same as for argon, as discussed in Sec. III A above. We thus note here only the differences from our calculations for argon.

One difference is that the phase function governing the asymptotic behavior of our final-state wave functions has the asymptotic behavior

$$\theta(l,k,r) \underset{r\rightarrow\infty}{\sim} kr-\tfrac{1}{2}\pi l \tag{56}$$

instead of that given in Eq. (50b). Both $\theta(l,k,r)$ and the amplitude $\zeta(l,k,r)$ [cf. Eq. (50)] have been calculated for our F^- wave functions using the procedure of Burgess.[46] The experimental[51] detachment energy for F^- is 3.399 eV as compared with the HF $2p$ orbital binding energy[40] of 4.921 eV. The experimental ionization energy[47] of F is 17.422 eV, so that the experimental energy to remove two $2p$ electrons from F^- is 20.821 eV, which is used in our evaluation of the final-state electron scattering interactions, as described in Sec. III A above. By comparison, the HF binding energy to remove two $2p$ electrons is 9.842 eV in the frozen-core approximation.

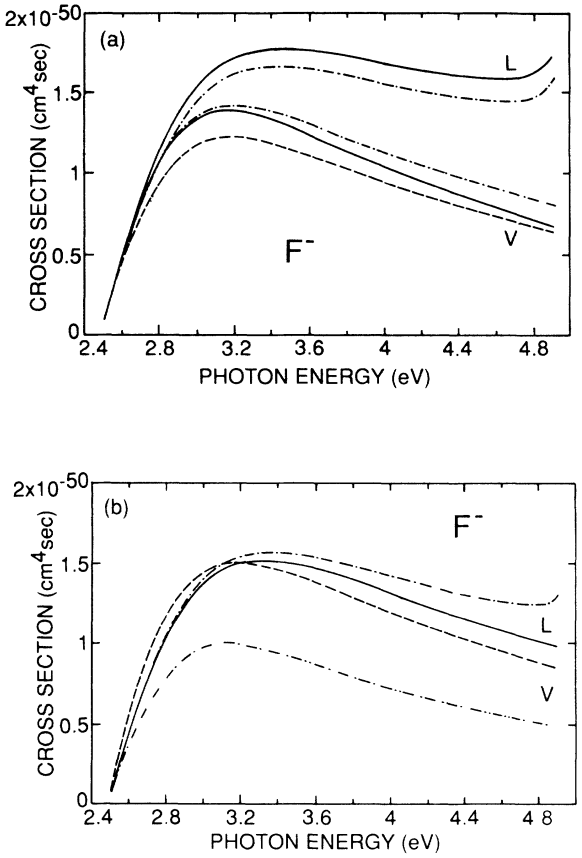

FIG. 7. Generalized two-photon total cross sections for the process $F^-2p^6(^1S)+2\gamma\rightarrow F\;2p^5(^2P)+e^-$ for linearly polarized incident light. L (V) indicates dipole length (velocity) results. (a) Solid curve, lowest-order $2p$-subshell HF results [process (1a) in Table I]. Dashed curve, including in addition the lowest-order $2s$-subshell HF results [process (1b) in Table I]. (Note that the dipole length dashed curve is indistinguishable from the dipole length solid curve.) Dash-dotted curve, including in addition intermediate-state interchannel interactions and ground-state correlations [processes (2) and (3) in Table I]. (b) Dash-dotted (L) and dash-double-dotted (V) curves, including all processes in Table I except for intermediate-state shake-up interactions [process (4) in Table I]. Solid (L) and dashed (V) curves, including all processes in Table I. (Note: HF binding energies were used to obtain all results shown.)

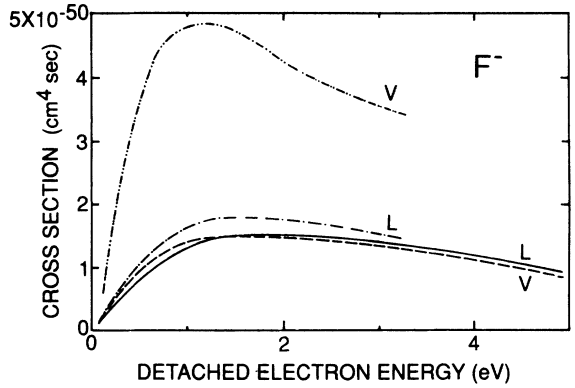

FIG. 8. Comparison of length (L) and velocity (V) results for the generalized two-photon detachment total cross section of F^- for linearly polarized incident light in the following two cases: (a) Using HF binding energies (solid and dashed curves). (b) Using experimental binding energies (dash-dotted and dash-double-dotted curves).

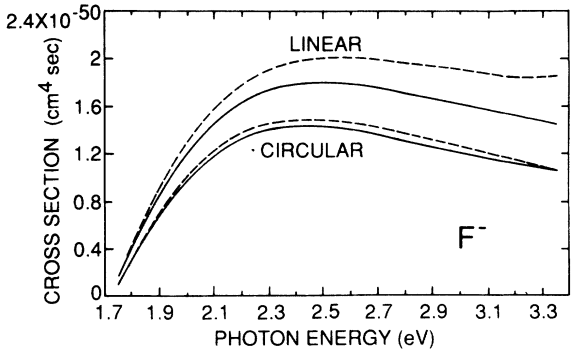

FIG. 10. Comparison of the total two-photon detachment cross sections for F^- for linearly and for circularly polarized incident light. Dashed curves, lowest-order HF results [process (1) in Table I]. Solid curves, results including all processes in Table I. All results shown were obtained using experimental binding energies and employing the dipole length formula.

A. Results for the two-photon detachment cross sections

The two-photon detachment cross section for F^- differs from that for Ar in not having any intermediate-state resonance structure and in having a zero value at threshold, in accordance with the Wigner threshold law.[52] We exhibit the role of the different electron correlation effects listed in Table I on the total two-photon detachment cross section for the case of linearly polarized light in Fig. 7. One sees that the dipole length results decrease monotonically as the various electron correlations listed in Table I are included in calculating the two-photon transition amplitude. At a photon energy of 4.8 eV the decrease of our curve including all correlation processes listed in Table I as compared to our HF result is almost 40%. In contrast, the various dipole velocity results alternately increase and decrease with the largest correction coming from the intermediate-state shake-up interactions [cf. process (4) in Table I]. Our final length and velocity curves are in reasonably good agreement.

The results shown in Fig. 7 were obtained using the theoretical (HF) binding energies. The discrepancies between the experimental and theoretical binding energies are much greater in F^- than in Ar. When we incorporate the experimental binding energies in our calculation in the way described in Sec. III A above, the dipole length cross section increases slightly, but the dipole velocity cross section increases by more than a factor of 3, as shown in Fig. 8. Such behavior of the velocity gauge results upon changing the energies used in our formulas is not entirely unexpected.[53] Because of this extreme sensitivity of the dipole velocity results, all further presentations of our results employ the dipole length formula and the experimental binding energies.

Our results for the partial two-photon detachment cross sections are shown in Fig. 9. For these dipole length results it is clear that electron correlation effects are negligible for the $f(^1D)$ channel, modest for the $p(^1D)$ channel, and quite large for the $p(^1S)$ channel. In the latter case, the intermediate-state shake-up process gives most of the total correction to the lowest-order HF results. These partial cross-section results explain the difference in the importance of electron correlations for the total cross sections for linearly and for circularly polarized light. As shown in Fig. 10, the effect of electron correlation is large for linearly polarized incident light but very modest for circularly polarized incident light. It should be noted that the $p(^1S)$ partial cross section does not contribute to the total cross section in the case of circularly polarized incident light.

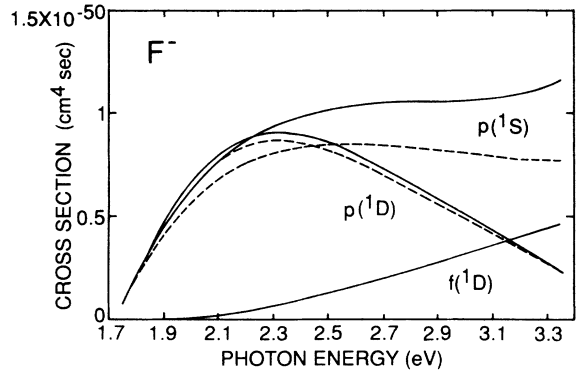

FIG. 9. Partial two-photon detachment cross sections for F^- for linearly polarized incident light [cf. Eq. (55)]. Solid curves, lowest-order HF results [process (1) in Table I]. Dashed curves, results including all processes in Table I. All results shown were obtained using experimental binding energies and employing the dipole length formula.

B. Comparisons with other theoretical and experimental results

There are two other theoretical calculations and one experimental measurement for the two-photon detachment cross section of F^-. Robinson and Geltman[18] have

presented dipole length central potential model results including the effect of a long-range polarization potential. More recently, Crance[19] has presented dipole length independent-electron-model results employing frozen-core HF wave functions (to describe the initial-state as well as the bound final-state electron orbitals) and both free-electron wave functions and HF wave functions to describe the detached electron. Most recently, Kwon *et al.*[27] have used a Nd:yttrium aluminum garnet (YAG) laser and an ion trap to obtain the first absolute measurement of the F^- two-photon detachment cross section.

Our results for the total two-photon detachment cross section for linearly polarized incident light are compared with these others in Fig. 11. Both our lowest-order HF results and our results including all correlation effects listed in Table I are in excellent agreement with the single experimental data point. Our HF results are roughly consistent with those of Crance.[19] Both the central potential model results[18] and the free-electron results,[19] however, are nearly a factor of 3 larger than our fully correlated results. The largest discrepancy is with the results of the central potential model calculation, which incorporates a long-range polarization potential. As noted in Ref. 21, however, and as discussed in detail elsewhere,[54] the detached electron may polarize the residual atomic core, leading to a reduction of the near threshold cross section. This effect has been neglected in the results of Ref. 18, thereby providing one explanation for the much larger predicted two-photon detachment cross section near threshold. The free-electron results[19] provide another explanation. Apparently the direct and exchange interactions of the detached electron with the residual core (which are included in the HF calculations) result in a large decrease in the predicted cross section near threshold. Furthermore, current experimental measurements[27] are capable of distinguishing between theories which incorporate such interactions and those which do not.

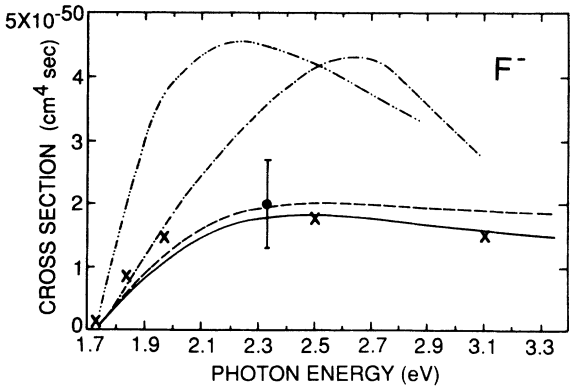

FIG. 11. Total two-photon detachment cross sections for F^- for linearly polarized incident light. Solid (dashed) curve, present dipole length results including all processes [only the lowest-order process (1)] in Table I and employing experimental binding energies. Dotted-dash curve, free-electron results of Crance (Ref. 19). Crosses, HF results of Crance (Ref. 19). Dash-double-dotted curve, Robinson and Geltman (Ref. 18). Experimental point, Kwon *et al.* (Ref. 27).

V. DISCUSSION AND CONCLUSIONS

We have presented two-photon ionization cross sections for the $3p$ subshell of argon and two-photon detachment cross sections for the $2p$ subshell of F^- in which the effects of electron correlations have been presented in detail. All of these effects have been calculated using variationally stable techniques to carry out the required summations over intermediate states implicitly. Such variationally stable techniques have permitted us to obtain much more reliable results for the intermediate-state resonance region in the case of argon than in a previous calculation by one of us.[12]

We have demonstrated here the importance of intermediate-state shake-up interactions for the $p(^1S)$ final-state channel cross sections. These interactions are particularly important for obtaining reasonable agreement of dipole length and velocity results. They also are responsible for the significantly lower total cross sections near threshold predicted here for argon as compared with the previous results of one of us,[12] with which we would otherwise agree from threshold up to the onset of the resonance region.

We conclude firstly that for all atoms or ions having a $p^6(^1S)$ initial configuration, the $p(^1S)$ final-state channel is the most sensitive to the effects of electron correlations. This is consistent with the discussion presented by Starace and Jiang.[12] Hence experimental measurements employing circularly polarized light are not as useful as those employing linearly polarized light so far as providing a test of theoretical handling of electron correlation effects. [This is so since the $p(^1S)$ channel is not excited in two-photon processes in the case of circularly polarized photons.] Conversely, theoretical predictions for the case of circularly polarized light, because they appear to be much less sensitive to electron correlation effects, can provide a much more reliable normalization for relative experimental measurements than predictions for linearly polarized light. Secondly, we conclude that for two-photon detachment of negative ions, the interaction of the detached electron with the residual atomic core must be described at least in the lowest-order HF approximation if agreement with experiment is to be obtained.

Finally, we have shown that the various theoretical predictions for the two-photon ionization cross section of argon differ significantly in the resonance region. We expect that our present variationally stable results are fairly reliable in this energy region. However, this expectation requires confirmation by other researchers.

ACKNOWLEDGMENTS

This work was supported in part by National Science Foundation Grant No. PHY-8908605.

APPENDIX

We give here for reference those angular factors defined in the text, most of which cannot be found in

standard references.[55] All angular factors were calculated analytically using graphical techniques.[56,57]

1. Equation (16) coefficients

The coefficients defined in Eq. (16) are given by

$$a_{l_1}(l,L)=(3[L])^{1/2}(l\|C^1\|l_1)\begin{Bmatrix}1 & L & 1\\ l & l_1 & 1\end{Bmatrix} \tag{A1}$$

and

$$b_{l_1}=(2)^{1/2}(l_1\|C^1\|1)\ , \tag{A2}$$

where l_1 may have the values 0 or 2.

The operators v_{sd} and v_{ds} defined in Eq. (16) are given in terms of their matrix elements,

$$\langle\lambda_d^f|v_{ds}|\lambda_s^i\rangle=-(\tfrac{8}{9})^{1/2}R^1(\lambda_d^f np,\lambda_s^i np)+(\tfrac{2}{25})^{1/2}R^2(\lambda_d^f np,np\lambda_s^i) \tag{A3}$$

and

$$\langle\lambda_s^f|v_{sd}|\lambda_d^i\rangle=\langle\lambda_d^i|v_{ds}|\lambda_s^f\rangle\ . \tag{A4}$$

The matrix element on the right in Eq. (A4) is equal to that given in Eq. (A3) upon making the replacements $i\rightarrow f$ and $f\rightarrow i$.

2. Equation (22) coefficients

The coefficients defined in Eq. (22) are given by

$$A(k,l_1,l_2,l,L)=(6[L])^{1/2}(l\|C^1\|l_1)(1\|C^1\|l_2)(l_2\|C^k\|1)(l_1\|C^k\|1)\begin{Bmatrix}l_1 & 1 & 1\\ L & l & 1\end{Bmatrix}\left[(-1)^k\tfrac{2}{3}\delta_{k1}+\begin{Bmatrix}1 & l_2 & k\\ 1 & l_1 & 1\end{Bmatrix}\right]\ . \tag{A5}$$

3. Equation (35) coefficients

The coefficients defined in Eq. (35) are given by

$$\begin{aligned}B(k,l_1,l,L)=&\,4(6)^{1/2}(l\|C^k\|1)(1\|C^k\|1)(1\|C^1\|l_1)(l_1\|C^1\|1)[L]^{1/2}\begin{Bmatrix}1 & l_1 & 1\\ 1 & L & 1\end{Bmatrix}\\ &\times\sum_{(\tilde{L}\tilde{S})}\sum_{(\tilde{L}'\tilde{S})}\sum_{L'S'}(-1)^{1+L'+\tilde{L}'}[\tilde{L}][\tilde{L}'][2-(-1)^{\tilde{L}}]^{1/2}[2-(-1)^{\tilde{L}'}]^{1/2}\\ &\times(p^4(\tilde{L}\tilde{S})\{|p^3(L'S')\rangle\langle p^3(L'S')|\}p^4(\tilde{L}'\tilde{S}))\begin{Bmatrix}1 & \tilde{L} & L'\\ \tilde{L}' & 1 & k\end{Bmatrix}\\ &\times\begin{Bmatrix}1 & \tilde{L} & 1\\ \tilde{L}' & l & k\end{Bmatrix}\begin{Bmatrix}\tilde{L}' & 1 & l\\ L & 1 & 1\end{Bmatrix}\\ &-\delta_{l1}(6)^{1/2}(1\|C^1\|l_1)(l_1\|C^1\|1)[L]^{1/2}\begin{Bmatrix}1 & l_1 & 1\\ 1 & L & 1\end{Bmatrix}[6\delta_{k0}-\tfrac{1}{3}(1\|C^k\|1)^2](6\delta_{L0}-1)\ .\end{aligned} \tag{A6}$$

4. Equation (42) coefficients

The coefficients defined in Eq. (42) are given by

$$\begin{aligned}C(k,l_1,l_2,l,L)=&\,(6)^{1/2}(l\|C^k\|l_1)(1\|C^k\|l_2)(l_2\|C^1\|1)(l_1\|C^1\|1)[L]^{1/2}(-1)^k\\ &\times\left[\tfrac{2}{3}\delta_{k1}\begin{Bmatrix}l_1 & 1 & 1\\ L & 1 & l\end{Bmatrix}+(-1)^{L+1}\begin{Bmatrix}l & l_2 & 1\\ 1 & L & 1\end{Bmatrix}\begin{Bmatrix}l & l_2 & 1\\ 1 & l_1 & k\end{Bmatrix}\right]\ .\end{aligned} \tag{A7}$$

5. Equation (47) coefficients

The coefficients defined in Eq. (47) are given by

$$d(k,l_1,l_2)=(l_1\|C^1\|1)^{-1}(1\|C^1\|l_2)(l_1\|C^k\|1)(l_2\|C^k\|1)\left[\tfrac{2}{3}\delta_{k1}(-1)^k+\begin{Bmatrix}1 & l_2 & k\\ 1 & l_1 & 1\end{Bmatrix}\right]\ . \tag{A8}$$

These coefficients are equal to $A(k,l_1,l_2,l,L)/(a_{l_1}b_{l_1})$, where A is given by Eq. (A5), a_{l_1} is given by Eq. (A1), and b_{l_1} is given by Eq. (A2).

[1]See, e.g., the following collections of review articles and conference proceedings: *Multiphoton Ionization of Atoms,* edited by S. L. Chin and P. Lambropoulos (Academic, New York, 1984); Proceedings of a Conference on *Multielectron Excitations in Atoms, Seattle, 1986,* edited by W. E. Cooke and T. J. McIlrath [J. Opt. Soc. Am. **4**, 701 (1987)]; *Multiphoton Processes,* edited by S. J. Smith and P. L. Knight (Cambridge University Press, New York, 1988); P. Agostini, in *Fundamental Processes of Atomic Dynamics,* Vol. 181 of *NATO Advanced Study Institute Series B: Physics,* edited by J. S. Briggs, H. Kleinpoppen, and H. O. Lutz (Plenum, New York, 1988), pp. 483–511; J. L. Dehmer, S. T. Pratt, M. A. O'Halloran, and F. S. Tomkins, in *ibid.*, pp. 513–540; A. Giusti-Suzor, in *ibid.*, pp. 217–234.

[2]A. L'Huillier, L. A. Lompré, G. Mainfray, and C. Manus, Phys. Rev. Lett. **48**, 1814 (1982); Phys. Rev. A **27**, 2503 (1983); J. Phys. B **16**, 1363 (1983); L. A. Lompré, A. L'Huillier, G. Mainfray, and J. Y. Fan, J. Phys. B **17**, L817 (1984).

[3]T. S. Luk, H. Pummer, K. Boyer, M. Shahidi, H. Egger, and C. K. Rhodes, Phys. Rev. Lett. **51**, 110 (1983); C. K. Rhodes, Science **220**, 1345 (1985).

[4]P. Lambropoulos, Phys. Rev. Lett. **55**, 2141 (1985).

[5]G. A. Victor, Proc. Phys. Soc. London **91**, 825 (1967).

[6]M. S. Pindzola and H. P. Kelly, Phys. Rev. A **11**, 1543 (1975).

[7]B. Ritchie, Phys. Rev. A **16**, 2080 (1977).

[8]E. J. McGuire, Phys. Rev. A **24**, 835 (1981).

[9]R. Moccia, N. K. Rahman, and A. Rizzo, J. Phys. B **16**, 2737 (1983).

[10]A. L'Huillier, L. Jönsson, and G. Wendin, Phys. Rev. A **33**, 3938 (1986).

[11]P. Gangopadhyay, X. Tang, P. Lambropoulos, and R. Shakeshaft, Phys. Rev. A **34**, 2998 (1986).

[12]A. F. Starace, and T.-F. Jiang, Phys. Rev. A **36**, 1705 (1987).

[13]A. L'Hullier and G. Wendin, J. Phys. B **20**, L37 (1987); Phys. Rev. A **36**, 4747 (1987).

[14]K. C. Kulander, Phys. Rev. A **36**, 2726 (1987); **38**, 778 (1988).

[15]A. L'Huillier, X. Tang, and P. Lambropoulos, Phys. Rev. A **39**, 1112 (1989).

[16]M. Crance and M. Aymar, J. Phys. B **18**, 3529 (1985).

[17]M. G. J. Fink and P. Zoller, J. Phys. B **18**, L373 (1985).

[18]E. J. Robinson and S. Geltman, Phys. Rev. **153**, 4 (1967).

[19]M. Crance, J. Phys. B **20**, 6553 (1987); **21**, 3559 (1988).

[20]A. L'Huillier and G. Wendin, J. Phys. B **21**, L247 (1988).

[21]T.-F. Jiang and A. F. Starace, Phys. Rev. A **38**, 2347 (1988).

[22]J. L. Dehmer, S. T. Pratt, and P. M. Dehmer, Phys. Rev. A **36**, 4494 (1987).

[23]S. T. Pratt, P. M. Dehmer, and J. L. Dehmer, Phys. Rev. A **35**, 3793 (1987).

[24]C. Y. Tang, P. G. Harris, A. H. Mohagheghi, H. C. Bryant, C. R. Quick, J. B. Donahue, R. A. Reeder, S. Cohen, W. W. Smith, and J. E. Stewart, Phys. Rev. A **39**, 6068 (1989).

[25]R. Trainham, G. D. Fletcher, and D. J. Larson, J. Phys. B **20**, L777 (1987).

[26]C. Blondel, R.-J. Champeau, M. Crance, A. Crubellier, C. Delsart, and D. Marinescu, J. Phys. B **22**, 1335 (1989).

[27]N. Kwon, P. S. Armstrong, T. Olsson, R. Trainham, and D. J. Larson, Phys. Rev. A **40**, 676 (1989).

[28]R. M. Sternheimer, Phys. Rev. **84**, 244 (1951).

[29]A. Dalgarno and J. T. Lewis, Proc. R. Soc. London, Ser. A **233**, 70 (1955).

[30]T. N. Chang and R. T. Poe, J. Phys. B **9**, L311 (1976); Phys. Rev. A **16**, 606 (1977).

[31]T. P. Das and R. Bersohn, Phys. Rev. **102**, 733 (1956).

[32]A. Dalgarno and J. T. Lewis, Proc. Phys. Soc. London, Ser. A **69**, 628 (1956).

[33]J. Nuttal and H. L. Cohen, Phys. Rev. **188**, 1542 (1969).

[34]B. Gao and A. F. Starace, Phys. Rev. Lett. **61**, 404 (1988); Phys. Rev. A **39**, 4550 (1989).

[35]C. Pan, B. Gao, and A. F. Starace, Bull. Am. Phys. Soc. **34**, 1384 (1989).

[36]W. L. Peticolas, R. Norris, and K. E. Rieckhoff, J. Chem. Phys. **42**, 4164 (1965), Appendix.

[37]C. Froese Fischer, *The Hartree-Fock Method for Atoms* (Wiley, New York, 1977).

[38]A. F. Starace, in *Corpuscles and Radiation in Matter I,* Vol. 31 of *Handbuch der Physik,* edited by W. Mehlhorn (Springer, Berlin, 1982), Secs. 16 and 17 and references therein.

[39]B. Gao, C. Pan, C. R. Liu, and A. F. Starace, J. Opt. Soc. Am. B **7**, 622 (1990).

[40]E. Clementi and C. Roetti, At. Data Nucl. Data Tables **14**, 177 (1974).

[41]L. M. Frantz, R. L. Mills, R. G. Newton, and A. M. Sessler, Phys. Rev. Lett. **1**, 340 (1958).

[42]B. A. Lippmann, M. H. Mittleman, and K. M. Watson, Phys. Rev. **116**, 920 (1959).

[43]R. T. Pu and E. S. Chang, Phys. Rev. **151**, 31 (1966).

[44]H. J. Silverstone and M. L. Yin, J. Chem. Phys. **49**, 2026 (1968).

[45]S. Huzinaga and C. Arnau, Phys. Rev. A **1**, 1285 (1970).

[46]A. Burgess, Proc. Phys. Soc. London **81**, 442 (1963).

[47]C. E. Moore, *Ionization Potentials and Ionization Limits Derived from the Analyses of Optical Spectra,* Natl. Bur. Stand. Ref. Data Ser., Natl. Bur. Stand. (U.S.) Circ. No. 34 (U.S. GPO, Washington, D.C., 1970), p. 6b.

[48]A. L'Huillier and G. Wendin, Phys. Rev. A **36**, 5632 (1987).

[49]P. Lambropoulos, Adv. At. Mol. Phys. **12**, 87 (1976).

[50]U. Fano, Phys. Rev. **124**, 1866 (1961).

[51]H. Hotop and W. C. Lineberger, J. Phys. Chem. Ref. Data **4**, 539 (1975).

[52]E. P. Wigner, Phys. Rev. **73**, 1002 (1948).

[53]S. Olariu, I. Popescu, and C. B. Collins, Phys. Rev. D **20**, 3095 (1979).

[54]D. W. Norcross, Phys. Rev. A **7**, 606 (1973), and references therein.

[55]J. C. Slater, *Quantum Theory of Atomic Structure* (McGraw-Hill, New York, 1960), Vol. II, Appendix 21.

[56]J. S. Briggs, Rev. Mod. Phys. **43**, 189 (1971).

[57]A. P. Yutsis, I. B. Levinson, and V. V. Vanagas, *The Theory of Angular Momentum* (Israel Program for Scientific Translation, Washington, D.C., 1962).